ACS APPLIED NANO MATERIALS

www.acsanm.org Article

Assembly of Pt Nanoparticles on Graphitized Carbon Nanofibers as Hierarchically Structured Electrodes

Nejc Hodnik,* Luigi Romano,* Primož Jovanovič, Francisco Ruiz-Zepeda, Marjan Bele, Filippo Fabbri, Luana Persano, Andrea Camposeo, and Dario Pisignano

Cite This: *ACS Appl. Nano Mater.* 2020, 3, 9880−9888 Read Online

ACCESS | Metrics & More | Article Recommendations | Supporting Information

ABSTRACT: Carbon-based nanofibers decorated with metallic nanoparticles (NPs) as hierarchically structured electrodes offer significant opportunities for use in low-temperature fuel cells, electrolyzers, flow and air batteries, and electrochemical sensors. We present a facile and scalable method for preparing nanostructured electrodes composed of Pt NPs on graphitized carbon nanofibers. Electrospinning directly addresses the issues related to large-scale production of Pt-based fuel cell electrocatalysts. Through precursors containing polyacrylonitrile and Pt salt electrospinning along with an annealing protocol, we obtain approximately 180 nm thick graphitized nanofibers decorated with approximately 5 nm Pt NPs. By *in situ* annealing scanning transmission electron microscopy, we qualitatively resolve and quantitatively analyze the unique dynamics of Pt NP formation and movement. Interestingly, by very efficient thermal-induced segregation of all Pt from the inside to the surface of the nanofibers, we increase overall Pt utilization as electrocatalysis is a surface phenomenon. The obtained nanomaterials are also investigated by spatially resolved Raman spectroscopy, highlighting the higher structural order in nanofibers upon doping with Pt precursors. The rationalization of the observed phenomena of segregation and ordering mechanisms in complex carbon-based nanostructured systems is critically important for the effective utilization of all metal-containing catalysts, such as electrochemical oxygen reduction reactions, among many other applications.

KEYWORDS: *electrocatalysis, in situ annealing STEM, platinum nanoparticles, electrodes, electrospinning*

1. INTRODUCTION

Unsustainable methods to obtain utilizable energy are causing global warming because of the rising CO_2 concentration in the earth's atmosphere.[1] In order to decrease the burning of fossil fuels, the accelerated implementation and development of sustainable energy sources is urgently needed.[2] One of the possible solutions is provided by exploiting hydrogen produced from renewables such as solar and wind to store electrical energy in chemical bonds.[3] In this respect, fuel cells play an important role in the conversion of hydrogen back into electricity. The core component and the current bottleneck for efficient (activity), reliable (stability) operation and economic viability is the electrocatalyst for the oxygen reduction reaction (ORR).[4] In proton-exchange membrane fuel cells, this reaction relies on expensive and rare raw materials, particularly platinum (Pt), deposited on high-surface-area carbon supports.[4] Therefore, an optimal utilization, namely, effective deployment of Pt, is of paramount importance. This can be accomplished by increasing the available active surface and the utilization of an appropriate carbon-based support during the fabrication of the nanostructures. The optimal size of Pt nanoparticles (NPs) for the use in a low-temperature fuel cell is between 3 and 5 nm.[4,5] Unfortunately, many techniques for synthesizing metal NPs such as a polyol, colloidal, water−oil emulsion, sol−gel, hydrothermal, galvanic displacement, and so forth[6−8] involve several different processing steps for deposition or formation on conductive supports, thus making the production complex. A robust method to produce NPs for electrocatalysis already integrated into a nanocomposite with the appropriate carbon support, which would be based on straightforward procedures as well as on a limited number of processing steps, is therefore much more suitable for the scale-up.[9]

Electrospinning techniques allow quasi-one-dimensional mesostructured organic, inorganic, and hybrid nanomaterials, potentially with controlled hierarchical features, to be obtained from electrified polymer solutions with a sufficient amount of macromolecular entanglements.[10−13] Electrochemical applications range from fuel cells to electrolyzers, flow batteries, air batteries, electrochemical sensors, capacitors, and water cleaning.[13−17] In particular, the combination of nanofibers

Received: July 17, 2020
Accepted: September 1, 2020
Published: September 1, 2020

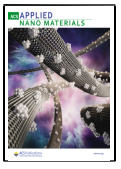

https://dx.doi.org/10.1021/acsanm.0c01945
ACS Appl. Nano Mater. 2020, 3, 9880−9888

Scheme 1. Procedures for the Synthesis/Fabrication of Pt NPs Deposited on the Graphitized Carbon Nanofibers (Hierarchically Structured Electrodes)

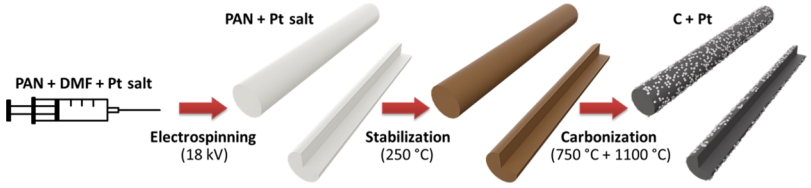

with functional NPs used as dopants gained continuously increasing interest,[17] which has immediate implications on the realization of thermally treated, electrospun Pt−carbon nanocomposites. Organic fibers can be based on polyacrylonitrile (PAN), cellulose, or epoxy resins, which are used as precursors to produce conductive, carbon-based filaments and supports by thermal treatment.[18−20] In this framework, PAN is a popular polymer because it is an affordable precursor and easily electrospun, which is why it is also used to make carbon fibers at an industrial scale.[21] In addition, other electrospun supports, including oxides, can be exploited for Pt catalysts;[22,23] however, many of them still have low electrical conductivity and are easy to degrade. As an alternative, electrospun Pt-based nanofibers without supports have been produced; however, they result in particularly low Pt utilization.[24,25]

Overall, electrospun Pt/C electrocatalysts can be obtained by either *in situ* or *ex situ* synthesis, that is, by producing carbon fibers either simultaneously with Pt NPs or prior to Pt-NP deposition. For the latter case, Pt can be deposited physically as well as by some chemical steps,[26,27] including electrodeposition.[17] In many of these methods, it is difficult to achieve a homogeneous deposition without the presence of agglomerates. For instance, electrochemical techniques show limitations in terms of particle size distribution and uneven surface coverage.[26,28,29] Particles larger than 50 nm are generally obtained by this process, which is quite far from the sub 5 nm size range for optimal Pt utilization. These issues may be addressed to some extent by the novel process known as controlled cathodic corrosion, which exploits electrochemical biasing at low potentials to break down metallic NPs.[30] On the other hand, forming Pt NPs *in situ* can lead to significant enhancement of particle stability,[7,31] including more efficient charge-transfer dynamics.[32] Nevertheless, a challenge, in this case, is making Pt NPs properly available on carbon-active surfaces, without having them embedded inside the bulk carbon phase where they are inaccessible to reactants.[31,33,34] To date, exploring and studying these aspects has been complicated, on one hand, by no positive experimental evidence of such events that exist and, on the other hand, by the difficulty to observe *in situ* the Pt-NP synthesis dynamics. This unexplored phenomenon presents a challenge to be investigated because of the complexity that implies monitoring the annealing process at the level of an individual fiber at high-temperature conditions.

Here, we applied *in situ* scanning transmission electron microscopy (STEM) to track the real-time dynamics of the annealing process at the scale of a single Pt-decorated carbon-based nanofiber. A Pt precursor is added to a polymer mixture before electrospinning, and 5 nm Pt NPs are obtained on the surface of graphitized nanofibers upon annealing. The process of Pt NP formation, growth, and segregation along with nanofiber shrinkage is characterized by *in situ* STEM. The resultant hybrid nanocomposite fibers are usable for active ORR three dimensional (3D)-structured Pt-based electrodes. The study of the NP dynamics formation from precursors and the subsequent segregation in carbon-based nanomaterials is highly relevant not only for the improved design of nanocomposites and electrochemical devices (and also other fields) but also for elaborating suitable models that describe how temperature affects the active surface of Pt-based electrodes.

2. EXPERIMENTAL SECTION

2.1. Preparation of Pt-Decorated Carbon-Based Nanofibers. The basic concept behind the fabrication of Pt-decorated graphitized nanofibers for use as free-standing electrodes is displayed in Figure S1 in the Supporting Information. Specifically, 80 mg of PAN (M_w = 150,000 g/mol, Sigma-Aldrich) is dissolved in 1 mL of *N*,*N*-dimethylformamide (Sigma-Aldrich). Tetraammineplatinum(II) nitrate ($[Pt(NH_3)_4](NO_3)_2$, Sigma-Aldrich) is also dissolved in the solution by keeping the Pt content constant at 10% w/w with respect to the polymer carbon. During electrospinning, the solution is pumped through a 27 gauge needle using a programmable syringe pump (Harvard Apparatus), with a flow rate of 15 μL/min. Nonwovens are electrospun in 40 min with an applied voltage of 18 kV, deposited on a copper target covered with a tin foil at a distance of 25 cm from the needle, and then gently peeled off. Nanofibers are stabilized in a muffle oven (250−300 °C, a ramp rate of 5 °C/min) in an air atmosphere for 1 h. Carbonization is performed in a customized vacuum furnace (Figure S2 in the Supporting Information, 10^{-6} to 10^{-7} Pa) by preheating nanofibers at a rate of 5 °C/min up to 750 °C, keeping the temperature stable for 30 min, and further heating up to 1100 °C for 1 h resulted in approximately 50% mass loss (making the expected final Pt content about 5% w/w). Experiments at lower temperatures (e.g., heating to 500 °C for 30 min and then to 800 °C for a further 1 h) are also carried out for assessing the effect of the thermal treatment on the obtained nanocomposites. For the sake of comparison, PAN solutions without Pt precursors are electrospun and thermally treated under the same process conditions. The whole synthesis/fabrication process is illustrated in Scheme 1.

2.2. Morphological and Structural Characterization. The composite materials are first inspected using an upright Olympus BX52 microscope (Olympus Life Science). Optical micrographs are acquired in the bright-field and dark-field modes through a 50× objective [a numerical aperture (NA) of 0.80]. Scanning electron microscopy (SEM) is performed using a field emission scanning electron microscope (Supra 35 VP Carl Zeiss, Germany). STEM is performed using a probe Cs-corrected scanning transmission electron microscope (JEOL ARM 200CF) operated at 80 kV. Scanning, spatially resolved Raman measurements (μ-Raman) are carried out with a Renishaw inVia spectrometer equipped with a confocal optical microscope and a 532 nm excitation laser. The spectral resolution of the system is 3 cm^{-1}. The μ-Raman spectra are recorded with a 50× objective (an NA of 0.8), a laser power of 1 mW, and an acquisition time of 5 s. The pixel size is 1 μm × 1 μm, which is comparable with the laser spot size.

2.3. Electrochemistry. A DropSens potentiostat (μStat 400 bipotentiostat/galvanostat) is used for cyclic voltammetry, with 0.1 M

https://dx.doi.org/10.1021/acsanm.0c01945
ACS Appl. Nano Mater. 2020, 3, 9880−9888

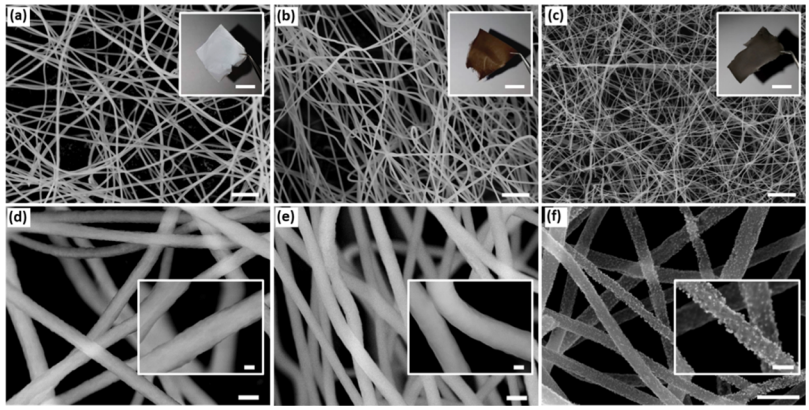

Figure 1. (a–c) SEM micrographs of Pt-loaded PAN nanofibers: (a) as-electrospun, (b) after stabilization at 250 °C in air, and (c) after subsequent heating up to 1100 °C in vacuum. Scale bars: 3 μm. Insets: corresponding sample photographs. Scale bars: 1 cm. (d–f) High-magnification SEM micrographs of as-electrospun (d), stabilized (e), and carbonized (f) nanofibers. Scale bars: 400 nm. Insets: zoom at the scale of a few fibers, allowing surface features to be appreciated. Scale bars: 100 nm.

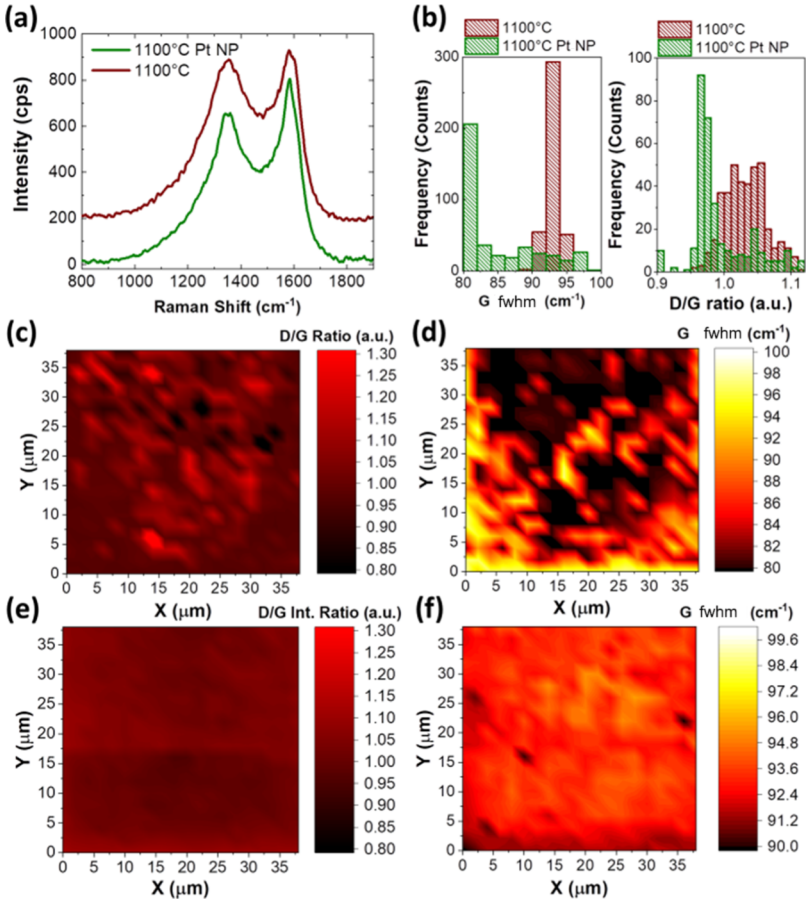

Figure 2. (a) Comparison of Raman spectra of thermally treated fibers with (green line) and without (red line) Pt NPs. Spectra are vertically shifted for better clarity. (b) Statistical analysis of the spectral width of the G mode and the D/G intensity ratio for the two materials. (c,d) D/G intensity ratio and G fwhm maps for the system with Pt NPs. (e,f) D/G intensity ratio and G fwhm maps for the system without Pt NPs.

H_2SO_4 as the electrolyte, an Ag/AgCl reference electrode (BASi), and a graphite rod as a counter electrode. The working electrode is the glassy carbon electrode on DropSens chips (screen-printed, Figure S3). Pt/C fibers (a sample size of ~5 × 3 mm^2) are fixed with a 3 μL drop of Nafion solution (diluted 1/50 with isopropanol). Fibers are treated with 10% oxygen plasma for 35 s to make them hydrophilic. The potential is scanned with 200 mV/s from −0.2 V to different upper potential values of 0.8, 1.0, 1.2, 1.4, and 1.6 V. The methanol oxidation reaction (MOR) is measured by the same protocol, with the addition of 1 M MeOH in the electrolyte.

2.4. ORR Measurements. The ORR activity of the realized nanocomposites is analyzed by using a three-electrode cell in a floating arrangement.[35] All the three electrodes (AgCl as the reference electrode, graphite rod as the counter electrode, and nanofibers as the working electrode) are placed in the same glass cell compartment. Nanofibers are used in a floating configuration, that is, they are placed on the surface of the electrolyte. To this aim, a polyether ether ketone

https://dx.doi.org/10.1021/acsanm.0c01945
ACS Appl. Nano Mater. 2020, 3, 9880–9888

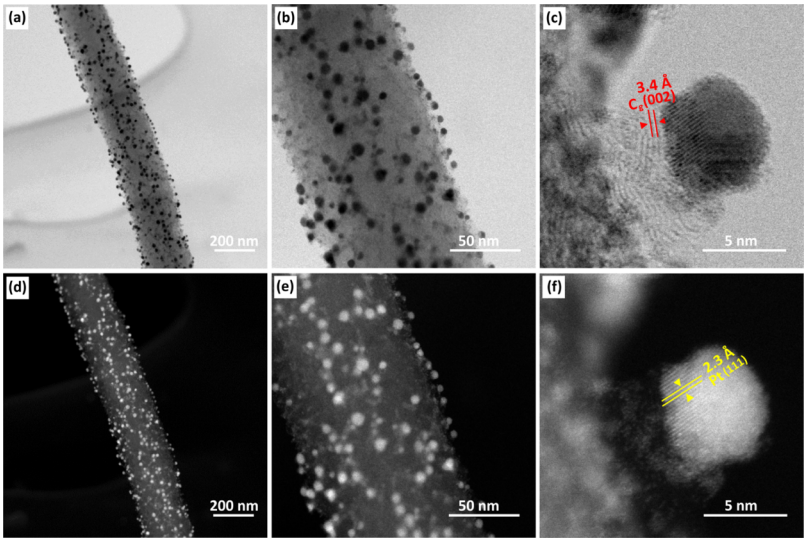

Figure 3. Bright-field (a–c) and annular dark-field (d–f) STEM micrographs with different magnifications of individual electrospun nanofibers annealed at 1100 °C, with Pt NPs. (c) Highlighted interplanar distance corresponding to C_g(002) planes of graphite (in red). (f) Highlighted interplanar distance corresponding to Pt(111) planes (yellow).

housing is designed, drilling holes to insert a gas pipe. This delivers oxygen to the surface of the working electrode (scheme in Figure S4). The pressures at the outlet of the so-connected oxygen tank are set at 1.5, 2.5, 3, and 4 bar for ORR polarization curve measurements.

2.5. *In Situ* Annealing STEM Analysis. Experiments are carried out using an *in situ* holder with a heating stage from Aduro Protochips Inc. The heating temperature on the specimen area is accurately controlled by providing an electrical signal to two electrodes using an external power supply. The *in situ* system uses disposable micro-electromechanical system chips with silicon nitride membranes as sample supports (Figure S5). Prior to *in situ* investigation, samples are ultrasonicated (Iskra Sonis 4) in ethanol for 20 min. Afterward, 2 μL of the suspension is pipetted on the silicon nitride membranes, the droplet is left to dry, and the chips are inspected under an optical microscope in order to check for the presence of nanofibrous samples on the examination area for performing STEM then. The temperature conditions applied in these experiments are changed in real time during measurements with linear ramps, and the samples are then kept at 1100 °C for 1 h. Within a large area containing fibers, identical sample regions are investigated *in situ* during experiments (screen-capture software Camtasia).[36]

3. RESULTS AND DISCUSSION

Electrospinning nanofibers with Pt precursors are highly advantageous compared to dispersing previously synthesized metal NPs in the polymer solution. Indeed, this favors the molecular flow which is critical to nanofiber formation because it does not lead to potential particle aggregation in the solution and consequent eventual needle clogging, and it does not significantly increase the viscoelastic behavior of pristine solutions.[37] This, in turn, determines the easy achievement of uniform distributions of NPs generated by the subsequent precursor decomposition in the polymer matrix, where macromolecules further limit aggregation effects. Figure 1a shows the SEM micrograph of as-electrospun nanofibers and a photograph of the corresponding whitish sample (inset). After stabilization by heating at 250 °C, nanofibers exhibit a brown color. Their morphology is displayed in Figure 1b. The temperature chosen for stabilization (Figure S6) depends on added Pt precursors. For instance, at 300 °C, the Pt-loaded fibers show severe crumbling and structural breaking (Figure S7). On the contrary, the effects of thermal treatment at 250 or 300 °C are substantially analogous on nanofibers without Pt precursors, as shown in Figures S8 and S9, respectively. These findings are likely related to Pt catalyzing carbon corrosion reaction (C to CO_2).[38] Figure 1c shows a SEM micrograph of free-standing fibers after the final thermal process up to 1100 °C. Fibers become black (inset of Figure 1c). Figure 1d–f shows high-magnification SEM micrographs of as-electrospun, stabilized, and carbonized nanofibers, respectively. The stabilized nanofibers retain well the pristine, smooth surface morphology, whereas carbonized nanofibers clearly show the presence of Pt NPs on their surface (inset of Figure 1f).

The corresponding dimensional analysis of nanofibers is reported in Figure S10. The average diameter (ϕ) of as-spun fibers is 270 nm, slightly reducing (by about 20 nm) following stabilization. After carbonization, the average diameter of the fibers is strongly reduced to ϕ = 130 nm, corresponding to an overall ∼50% shrinkage upon removal of non-carbon groups, which proceeds through the formation of different gases (e.g., carbon oxides, H_2O, H_2, NH_3, and so forth) during relevant heating.[39] Fibers without Pt precursors that have undergone identical thermal treatment do not show the presence of NPs (Figure S11) and exhibit a higher ultimate average diameter (160 nm) compared to fibers electrospun with Pt precursors.

μ-Raman experiments allow the effect of Pt on the graphitization of carbon nanofibers to be analyzed more in depth. Figure 2a shows Raman spectra of the carbonized fibers with (green line) and without (red line) Pt NPs. Both spectra exhibit D and G modes related to nanocrystalline graphite.[40] Comparing the G full width at half-maximum (fwhm) as well as the D/G intensity ratio provides information on the degrees of disorder and crystallinity in the analyzed materials. In particular, the D/G intensity ratio is strictly related to the concentration of defects and the disorder of nanocrystalline graphite. In the case of fibers with Pt NPs, the D/G intensity ratio upon annealing is 0.97, whereas it increases up to 1.04 for fibers without Pt NPs, suggesting that Pt NPs template a higher order in the nanographitic fibers (Figure 2b). Representative maps of the D/G intensity ratio and the G mode fwhm for fibers with and without NPs are shown in Figure 2c,d, and in Figure 2e,f, respectively. Distribution data

https://dx.doi.org/10.1021/acsanm.0c01945
ACS Appl. Nano Mater. 2020, 3, 9880–9888

for the measured G fwhm (91−92 and 81−83 cm^{-1} for fibers without Pt NPs and with Pt NPs, respectively) support the conclusion that the presence of the Pt NPs promotes crystallization of the fibers (Figure 2b).

The morphology and crystalline structure of both obtained Pt NPs and graphitic filaments are evidenced through STEM imaging (Figure 3). The Pt NPs are well distributed on the surface of nanofibers and present an average diameter of about 5 nm. By further quantitative analysis of the SEM and STEM images, we were able to extract the portion of the NPs that are on the surface of the fibers relative to the ones inside. As SEM detects particles on the front side surface and STEM also detects the ones in the bulk and other side surfaces, by comparing the quantification parameter of the Pt-NP concentration at the surface, namely, *C* (number of NPs per micrometer of the fiber surface; see the Supporting Information for the discussion, eqs S1−S4, and Figures S12−S15), we estimate that approximately 15% of particles are inside the fibers. This, however, does not necessarily mean that these particles are not accessible to the reaction as fibers do exhibit some porosity (Figure S16).

STEM imaging at high resolution allows the observation of the graphitic structure with the characteristic distance corresponding to the (002) plane[41] (marked in red in Figure 3c). Additionally, the typical Pt lattice distance in the NPs corresponds to (111) planes,[42] as highlighted in yellow in Figure 3f. Notably, in Figure 3c,f, a good Pt-to-carbon contact *via* embedment can be observed, which is beneficial for effective electrical coupling as well as increased stability (preventing particle detachment) in the obtained nanocomposite system.

These properties are also highlighted by electrochemical cyclic voltammetry (Figure 4), exploiting the high electrocatalytic activity of Pt toward methanol.[43] Although one can reveal Pt oxidation and reduction peaks (careful inspection of Figure 4a already reveals a Pt-oxide reduction peak in the negative scan at 0.3 V), MOR is much more pronounced, which is favored by using high concentrations of methanol in the electrolyte. The electrochemical current−voltage curves clearly show an MOR signal, which is absent in control experiments without methanol (Figure 4a).

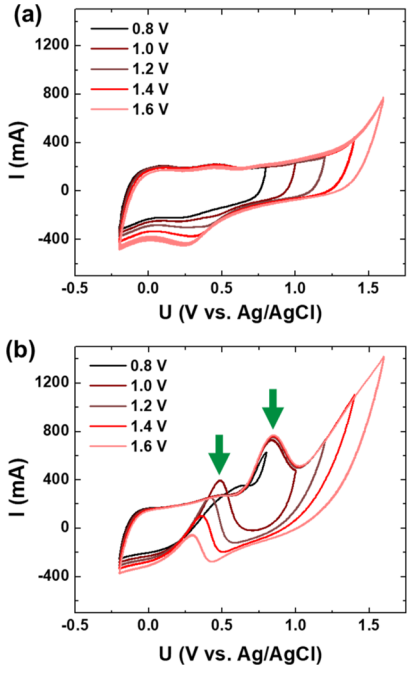

Figure 4. Cyclic voltammetry (200 mV/s) of nanofibers annealed at 1100 °C, with Pt NPs. Measurements are carried out without the addition of methanol (a) and with 1 M methanol added in 0.1 M H_2SO_4 (b). Green arrows in (b) highlight the peaks associated with methanol oxidation by Pt NPs.

Typical oxidation peaks, one in the forward and one in the backward scan, are highlighted by green arrows in Figure 4b. Increasing the upper potential limit distinctly shifts the cathodic peak to lower potentials and also decreases its height. This is due to the formation of more Pt oxide at higher upper potentials that is irreversibly reduced at lower potentials (Figure 4a also shows how the Pt-oxide reduction peak simultaneously increases and shifts to negative potentials from roughly 0.50−0.25 V).[44] As Pt is covered with oxide, it is not active for MOR. This is another indicator of the typical Pt electrocatalytic behavior toward MOR.[45]

Overall, electrochemistry confirms that Pt NPs are not embedded inside the fibers, being accessible to the electrolyte instead. Interestingly, when the annealing process is performed at 800 °C, no MOR signal is measured (Figure S17). This is in agreement with STEM analysis, revealing that in this case, Pt is largely sequestrated inside the fibers, with a much less uniform distribution of particles, and showing the presence of fibers without particles (Figure S18). These findings might indicate that fibers annealed at 800 °C are not porous, thus effectively preventing Pt−electrolyte interactions. We also notice that nanofibers annealed at lower temperatures show an average diameter larger than those carbonized at 1100 °C (Figure S19a). In this respect, a diameter reduction is to be related to the increase of the annealing temperature[46] because of the corresponding increase in carbon content and nanofiber densification.[47] As a consequence, the temperature also has a crucial role in the formation of nano-graphite features in the fibers.[48] Indeed, Raman analysis evidences that the fibers carbonized at lower temperatures show a relatively higher degree of disorder (Figure S19b), as highlighted by the higher D/G intensity ratio (D/G = 1.27), and less pronounced crystallinity, as suggested by the broader G peak (fwhm = 122 cm^{-1}).

In order to gain more insight into the annealing and Pt-NP segregation process, we perform extensive *in situ* STEM annealing experiments (Figure 5). This advanced characterization technique allows the annealing process to be monitored in real time, enabling the direct observation of the structural changes at the scale of an individual fiber while the temperature is increasing. Notably, no evident change in terms of Pt-NP formation can be detected during the preannealing step, from 250 °C (Figure 5a,d) to 750 °C (Figure 5b,e), whereas the appearance of NPs can be clearly appreciated during heating at 1100 °C (Figure 5c,f). Supporting videos are reported in the Supporting Information, which show the thermal evolution in the Pt-fiber morphology from 900 to 1100 °C (Video 1 in the Supporting Information) and the whole experiment that includes holding at 1100 °C for 1 h (Video 2), whereas significant frames at various time points during heating are shown in Figure S20. The clear onset of Pt-NP formation is found at a temperature between 900 and 930 °C (Figure S20). At 960 °C, Pt NPs start to form bigger particles that grow until the temperature of 1080 °C (marked with red and blue circles). Some particles already form at the

https://dx.doi.org/10.1021/acsanm.0c01945
ACS Appl. Nano Mater. 2020, 3, 9880−9888

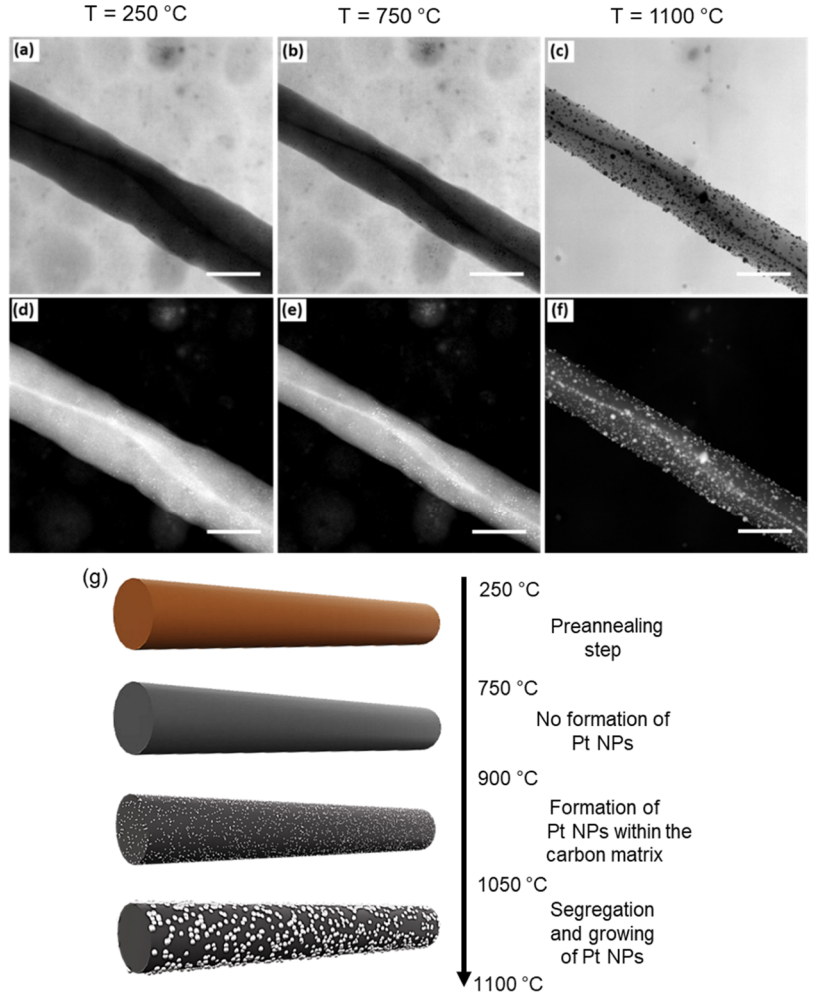

Figure 5. Snapshots of *in situ* STEM annealing experiments. Micrographs collected in bright field (a–c) and annular dark field (d–f) during three different stages of annealing of electrospun PAN nanofibers doped with Pt precursors: (a,d) stabilization, (b,e) heating at 750 °C, and (c,f) heating at 1100 °C. Scale bars: 200 nm. (g) Schematics of the corresponding Pt-NP synthesis and the surface segregation dynamics unveiled by STEM analysis.

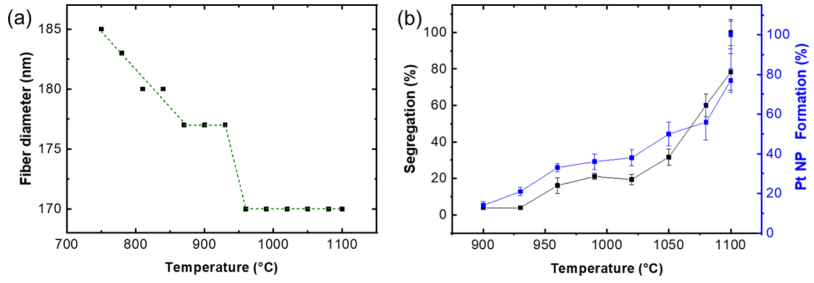

Figure 6. (a) Thermal evolution of the fiber diameter during annealing from 750 to 1100 °C; data from *in situ* STEM analysis. The dashed line is a guide for the eye. (b) Comparison of the NP segregation and formation dynamics at different temperatures.

surface of the fibers (marked by the yellow arrows). As the temperature increases up to 1100 °C, two events can be distinguished: (i) a sudden disappearance of the marked bigger NPs, followed by (ii) the appearance of new NPs on the nanofiber surface. The latter is highlighted in Figure S20c–f by yellow arrows along the fiber edge. The disappearance of certain NPs, which are presumably inside the nanofiber, is most likely related to the occurrence of the NPs on the surface. This dynamic process is fast as it occurs between 1050 and 1100 °C. In our opinion, the graphitization of the fiber is "forcing" Pt to segregate to the surface. Further studies are needed to explore and rationalize this interesting phenomenon. The subsequent formation and growth of Pt on the surface is a slow process, taking more than 30 min to reach a steady state (note that movies are increased by 64 times).

In situ STEM also allows for quantitative analysis by first monitoring the evolution of the fiber diameter during annealing. A single fiber shrinks from approximately 185–170 nm in the temperature range between 750 and 960 °C (Figure 6a). The shrinking at these temperatures could be correlated to the decrease in the content of nitrogen and hydrogen in the nanofibers, which is found to be relevant only

https://dx.doi.org/10.1021/acsanm.0c01945
ACS Appl. Nano Mater. 2020, 3, 9880–9888

at 1000 °C for PAN fibers without metal precursors.[49] This suggests that the polymer dehydrogenation and denitrogenation processes are also favored at a lower temperature by the presence of Pt. Second, by analyzing the evolution of the nanofiber in the recorded STEM *in situ* movie snapshots taken at different temperatures, we are able to monitor the change in the number of Pt NPs at the whole fiber as well as on the edge (Figure 6b and for more details, see the discussion, eqs S1−S4, and Figures S12−S15 in the Supporting Information). The particles formed on the edge are directly ascribed to the segregated ones. Therefore, by observing the dynamics of the edge particles compared to the dynamics on the whole fiber, we can see that Pt-NP formation and edge segregation show a similar trend at least until 1050 °C. This is likely the onset of the segregation phenomena, and therefore, the Pt segregation might become more effective at temperatures higher than 1050 °C (Figure 6b). Overall, the thermal evolution of Pt NPs is well outlined by *in situ* STEM analysis and is summarized in the scheme of Figure 5g. The analysis clearly evidences the segregation of Pt triggered by thermal annealing, which confines the NPs on the fiber surface.

The so-obtained 3D-structured Pt/C electrodes might be highly suitable as building blocks for newly designed electrochemical measuring cells (Figure S21a) based on a similar concept as those referred to as floating electrodes.[35] This allows for measuring high ORR current densities of the sample working electrode. In this configuration, free-standing, electrospun Pt/C electrodes are placed on the electrolyte surface, which enables fast mass transport of oxygen to the active sites. This is similar to low-temperature fuel cell arrangements where gas diffusion electrodes are sandwiched in a membrane electrode assembly. Novel ORR electrocatalysts are generally tested *via* thin-film rotating disc electrode (RDE) arrangements, where the working electrode is completely immersed in the electrolyte, and thus, oxygen solubility and mass transport might be slow. As a result, the RDE method only enables low current densities (up to ∼6 mA per cm_{geom}^2; geometric surface area),[50] which are not relevant for real fuel cell devices. With our floating electrode, we surpass RDE currents and overcome poor mass transport, measuring the ORR kinetics at significantly higher current densities, namely, above 40 mA/cm^2. Figure S21b shows four different ORR polarization curves, increasing in current density with the increase of feed O_2 gas pressure. Future experiments will aim at increasing Pt content in the nanostructured samples to values approaching those of state-of-the-art fuel cell catalysts (up to 50% w/w).[51] To avoid Pt synthesis, microwave-assisted chemical reduction could be used, which was shown to generate significantly more uniform nucleation and distribution of Pt NPs.[52] In addition, because of the mass transport and three-phase contact issues mentioned earlier, optimization will be done for further improving achievable current densities. In fact, because of a good graphite/Pt heterojunction observed in Figure 3c,f, the effect on the intrinsic activity should be explored.[53,54] Furthermore, we point out that current electrochemistry characterization is a proof of the concept at this stage, highlighting the potential future application of these materials. Further, efforts are needed in order to improve the electrochemistry methods (e.g., floating electrodes[55]) and thus the performance of these hierarchically structured electrodes.

4. CONCLUSIONS

We studied a facile and scalable method for preparing 3D-structured electrodes composed of Pt NPs on graphitized carbon nanofibers. The manufacturing approach directly addresses issues related to the large-scale production of Pt-based fuel cell electrocatalysts by exploiting electrospun fibers added with Pt precursors and knowing their thermal annealing behavior. The formation of NPs on the surface of the graphitized fibers is achieved by optimized and precisely controlled thermal annealing. The formation and segregation processes underneath are directly observed, tracked, and evaluated by *in situ* annealing STEM. We directly show that the Pt particle formation starts at approximately 900 °C and that Pt segregation is likely to set around 1050 °C. μ-Raman and electrochemistry experiments concur in rationalizing findings on the structural order and functional activity imparted by the Pt component. These electrode materials exhibit MOR and ORR at high current densities. Fundamental insights obtained in this study are useful for establishing new design rules for functional nanofibers and electrochemical devices.

■ ASSOCIATED CONTENT

Supporting Information

The Supporting Information is available free of charge at https://pubs.acs.org/doi/10.1021/acsanm.0c01945.

Scheme of the production of hierarchically structured fuel cell electrodes; photographs of PAN nanofibers carbonized in a vacuum furnace; photograph of DropSens chips used for cyclic voltammetry; floating electrode arrangement for ORR analysis; description of the *in situ* TEM annealing setup; Pt-loaded PAN nanofibers stabilized to 250 °C for 1 h in air; Pt-loaded PAN nanofibers stabilized to 300 °C for 1 h in air; PAN nanofibers stabilized to 250 °C for 1 h in air; PAN nanofibers stabilized to 300 °C for 1 h in air; histograms of diameter size for Pt-loaded nanofibers carbonized to 1100 °C; SEM analysis for PAN-carbonized fibers to 1100 °C without Pt NPs; snapshot of the particle counting on the SEM image performed by ImageJ; snapshot of the surface area calculation on the SEM image performed by ImageJ; snapshot of the particle counting on the TEM image performed by ImageJ; snapshot of the surface area calculation on the TEM image performed by ImageJ; SEM micrograph of individual electrospun nanofibers annealed at 1100 °C; cyclic voltammetry of Pt-loaded fibers annealed at 1100 °C; TEM micrographs of Pt-loaded nanofibers annealed at 800 °C; SEM and Raman analyses for Pt-loaded nanofibers annealed at 800 °C; *in situ* TEM micrographs of an individual fiber at different temperatures; and floating electrode setup and ORR polarization curves (PDF)

In situ STEM annealing movie of thermal evolution of the Pt-fiber morphology from 900 to 1100 °C (MP4)

In situ STEM annealing movie of the whole experiment that includes holding at 1100 °C for 1 h (MP4)

■ AUTHOR INFORMATION

Corresponding Authors

Nejc Hodnik − *NEST, Istituto Nanoscienze-CNR, I-56127 Pisa, Italy; Dipartimento di Matematica e Fisica "Ennio De Giorgi",*

https://dx.doi.org/10.1021/acsanm.0c01945
ACS Appl. Nano Mater. 2020, 3, 9880−9888

Università del Salento, I-73100 Lecce, Italy; Department of Materials Chemistry, National Institute of Chemistry, 1000 Ljubljana, Slovenia; orcid.org/0000-0002-7113-9769; Email: nejc.hodnik@ki.si

Luigi Romano − *NEST, Istituto Nanoscienze-CNR, I-56127 Pisa, Italy; Dipartimento di Matematica e Fisica "Ennio De Giorgi", Università del Salento, I-73100 Lecce, Italy; NEST, Scuola Normale Superiore, I-56127 Pisa, Italy;* Email: luigi.romano@sns.it

Authors

Primož Jovanovič − *Department of Materials Chemistry, National Institute of Chemistry, 1000 Ljubljana, Slovenia;* orcid.org/0000-0003-2477-3895

Francisco Ruiz-Zepeda − *Department of Materials Chemistry, National Institute of Chemistry, 1000 Ljubljana, Slovenia*

Marjan Bele − *Department of Materials Chemistry, National Institute of Chemistry, 1000 Ljubljana, Slovenia*

Filippo Fabbri − *NEST, Istituto Nanoscienze-CNR, I-56127 Pisa, Italy; Center for Nanotechnology Innovation@NEST, Istituto Italiano di Tecnologia, I-56127 Pisa, Italy*

Luana Persano − *NEST, Istituto Nanoscienze-CNR, I-56127 Pisa, Italy*

Andrea Camposeo − *NEST, Istituto Nanoscienze-CNR, I-56127 Pisa, Italy*

Dario Pisignano − *NEST, Istituto Nanoscienze-CNR, I-56127 Pisa, Italy; Dipartimento di Fisica, Università di Pisa, I-56127 Pisa, Italy;* orcid.org/0000-0003-3758-5199

Complete contact information is available at: https://pubs.acs.org/10.1021/acsanm.0c01945

Notes

The authors declare no competing financial interest.

■ ACKNOWLEDGMENTS

This study was supported by the Slovenian Research Agency for the research programme P2-0152 and P2-0393 and projects Z2-8161, N2-0106, and Z1-9165 and by the project "3D-Phys" (PRIN 2017PHRM8X) from the Italian Ministry of Education, University and Research. D.P. also acknowledges the support from the project PRA_2018_34 ("ANISE") from the University of Pisa. N.H. kindly acknowledges the Slovenian Research Agency for a fellowship to visit the ERC Grantee (D.P.) and project NC-0006. The vacuum furnace was acquired in the framework of the Apulia Regional Project "Networks of Public Research Laboratories", M.I.T.T.[13]

■ REFERENCES

(1) Solomon, S.; Plattner, G.-K.; Knutti, R.; Friedlingstein, P. Irreversible climate change due to carbon dioxide emissions. *Proc. Natl. Acad. Sci. U.S.A.* **2009**, *106*, 1704−1709.

(2) Chu, S.; Majumdar, A. Opportunities and challenges for a sustainable energy future. *Nature* **2012**, *488*, 294−303.

(3) Turner, J. A. Sustainable Hydrogen Production. *Science* **2004**, *305*, 972−974.

(4) Katsounaros, I.; Cherevko, S.; Zeradjanin, A. R.; Mayrhofer, K. J. J. Oxygen electrochemistry as a cornerstone for sustainable energy conversion. *Angew. Chem., Int. Ed.* **2014**, *53*, 102−121.

(5) Meier, J. C.; Galeano, C.; Katsounaros, I.; Witte, J.; Bongard, H. J.; Topalov, A. A.; Baldizzone, C.; Mezzavilla, S.; Schüth, F.; Mayrhofer, K. J. J. Design criteria for stable Pt/C fuel cell catalysts. *Beilstein J. Nanotechnol.* **2014**, *5*, 44−67.

(6) Xia, Y.; Xiong, Y.; Lim, B.; Skrabalak, S. E. Shape-controlled synthesis of metal nanocrystals: simple chemistry meets complex physics? *Angew. Chem., Int. Ed.* **2009**, *48*, 60−103.

(7) Bele, M.; Jovanovič, P.; Pavlišič, A.; Jozinović, B.; Zorko, M.; Rečnik, A.; Chernyshova, E.; Hočevar, S.; Hodnik, N.; Gaberšček, M. A highly active $PtCu_3$ intermetallic core-shell, multilayered Pt-skin, carbon embedded electrocatalyst produced by a scale-up sol-gel synthesis. *Chem. Commun.* **2014**, *50*, 13124−13126.

(8) Gatalo, M.; Bele, M.; Ruiz-Zepeda, F.; Šest, E.; Šala, M.; Kamšek, A. R.; Maselj, N.; Galun, T.; Jovanovič, P.; Hodnik, N.; Gaberšček, M. Double passivation water based galvanic displacement method for reproducible gram scale production of high performance Pt-alloy electrocatalysts. *Angew. Chem., Int. Ed.* **2019**, *131*, 13400−13404.

(9) Debe, M. K. Electrocatalyst approaches and challenges for automotive fuel cells. *Nature* **2012**, *486*, 43−51.

(10) Reneker, D. H.; Chun, I. Nanometre diameter fibres of polymer, produced by electrospinning. *Nanotechnology* **1996**, *7*, 216.

(11) Pisignano, D. *Polymer Nanofibers*; Royal Society of Chemistry: Cambridge, U.K., 2013.

(12) Cavaliere, S. *Electrospinning for Advanced Energy and Environmental Applications*; CRC Press: Boca Raton, FL, 2015.

(13) Greiner, A.; Wendorff, J. H. Electrospinning: a fascinating method for the preparation of ultrathin fibers. *Angew. Chem., Int. Ed.* **2007**, *46*, 5670−5703.

(14) Tang, H.; Chen, W.; Wang, J.; Dugger, T.; Cruz, L.; Kisailus, D. Electrocatalytic N-doped graphitic nanofiber−metal/metal oxide nanoparticle composites. *Small* **2018**, *14*, 1703459.

(15) Chen, H.; He, J.; Li, Y.; Luo, S.; Sun, L.; Ren, X.; Deng, L.; Zhang, P.; Gao, Y.; Liu, J. Hierarchical CuO_x−Co_3O_4 heterostructure nanowires decorated on 3D porous nitrogen-doped carbon nanofibers as flexible and free-standing anodes for high-performance lithium-ion batteries. *J. Mater. Chem. A* **2019**, *7*, 7691−7700.

(16) Xu, L.; Zhang, L.; Cheng, B.; Yu, J. Rationally designed hierarchical $NiCo_2O_4$−C@$Ni(OH)_2$ core-shell nanofibers for high performance supercapacitors. *Carbon* **2019**, *152*, 652−660.

(17) Zhang, C.-L.; Yu, S.-H. Nanoparticles meet electrospinning: recent advances and future prospects. *Chem. Soc. Rev.* **2014**, *43*, 4423−4448.

(18) Buchmeiser, M. R.; Muks, E.; Schowner, R.; Frank, E.; Hageroth, U.; Henzler, S.; Spörl, J.; Ota, A.; Beyer, R.; Müller, A. Structure evolution in all-aromatic, poly(p-phenylene-vinylene)-derived carbon fibers. *Carbon* **2019**, *144*, 659−665.

(19) Demiroğlu Mustafov, S.; Mohanty, A. K.; Misra, M.; Seydibeyoğlu, M. Ö. Fabrication of conductive Lignin/PAN carbon nanofibers with enhanced graphene for the modified electrodes. *Carbon* **2019**, *147*, 262−275.

(20) Sharma, C. S.; Sharma, A.; Madou, M. Multiscale carbon structures fabricated by direct micropatterning of electrospun mats of SU-8 photoresist nanofibers. *Langmuir* **2010**, *26*, 2218−2222.

(21) Rahaman, M. S. A.; Ismail, A. F.; Mustafa, A. A review of heat treatment on polyacrylonitrile fiber. *Polym. Degrad. Stab.* **2007**, *92*, 1421−1432.

(22) Nabil, Y.; Cavaliere, S.; Harkness, I. A.; Sharman, J. D. B.; Jones, D. J.; Rozière, J. Novel niobium carbide/carbon porous nanotube electrocatalyst supports for proton exchange membrane fuel cell cathodes. *J. Power Sources* **2017**, *363*, 20−26.

(23) Cavaliere, S.; Subianto, S.; Chevallier, L.; Jones, D. J.; Rozière, J. Single step elaboration of size-tuned Pt loaded titania nanofibres. *Chem. Commun.* **2011**, *47*, 6834−6836.

(24) Higgins, D. C.; Wang, R.; Hoque, M. A.; Zamani, P.; Abureden, S.; Chen, Z. Morphology and composition controlled platinum−cobalt alloy nanowires prepared by electrospinning as oxygen reduction catalyst. *Nano Energy* **2014**, *10*, 135−143.

(25) Kim, J. M.; Joh, H.-I.; Jo, S. M.; Ahn, D. J.; Ha, H. Y.; Hong, S.-A.; Kim, S.-K. Preparation and characterization of Pt nanowire by electrospinning method for methanol oxidation. *Electrochim. Acta* **2010**, *55*, 4827−4835.

(26) Wang, R.; Higgins, D. C.; Lee, D. U.; Prabhudev, S.; Hassan, F. M.; Chabot, V.; Lui, G.; Jiang, G.; Choi, J.-Y.; Rasenthiram, J.; Botton,

G.; Chen, Z.; Chen, Z. Biomimetic design of monolithic fuel cell electrodes with hierarchical structures. *Nano Energy* **2016**, *20*, 57−67.
(27) Wang, Y.; Li, G.; Jin, J.; Yang, S. Hollow porous carbon nanofibers as novel support for platinum-based oxygen reduction reaction electrocatalysts. *Int. J. Hydrogen Energy* **2017**, *42*, 5938−5947.
(28) Ercolano, G.; Farina, F.; Cavaliere, S.; Jones, D. J.; Rozière, J. Towards ultrathin Pt films on nanofibres by surface-limited electrodeposition for electrocatalytic applications. *J. Mater. Chem. A* **2017**, *5*, 3974−3980.
(29) Aboagye, A.; Elbohy, H.; Kelkar, A. D.; Qiao, Q.; Zai, J.; Qian, X.; Zhang, L. Electrospun carbon nanofibers with surface-attached platinum nanoparticles as cost-effective and efficient counter electrode for dye-sensitized solar cells. *Nano Energy* **2015**, *11*, 550−556.
(30) Vanrenterghem, B.; Hodnik, N.; Bele, M.; Šala, M.; Amelinckx, G.; Neukermans, S.; Zaplotnik, R.; Primc, G.; Mozetič, M.; Breugelmans, T. Increase of electrodeposited catalyst stability via plasma grown vertically oriented graphene nanoparticle movement restriction. *Chem. Commun.* **2017**, *53*, 9340−9343.
(31) An, G.-H.; Ahn, H.-J.; Hong, W.-K. Electrochemical properties for high surface area and improved electrical conductivity of platinum-embedded porous carbon nanofibers. *J. Power Sources* **2015**, *274*, 536−541.
(32) Alonso-Vante, N. Photocatalysis an enhancer of electrocatalytic process. *Curr. Opin. Electrochem.* **2018**, *9*, 114−120.
(33) Yang, T.; Du, M.; Zhu, H.; Zhang, M.; Zou, M. Immobilization of Pt nanoparticles in carbon nanofibers: bifunctional catalyst for hydrogen evolution and electrochemical sensor. *Electrochim. Acta* **2015**, *167*, 48−54.
(34) Wang, J.; Chen, J. W.; Chen, J. D.; Zhu, H.; Zhang, M.; Du, M. L. Designed synthesis of size-controlled Pt−Cu alloy nanoparticles encapsulated in carbon nanofibers and their high efficient electrocatalytic activity toward hydrogen evolution reaction. *Adv. Mater. Interfaces* **2017**, *4*, 1700005.
(35) Zalitis, C. M.; Kramer, D.; Kucernak, A. R. Electrocatalytic performance of fuel cell reactions at low catalyst loading and high mass transport. *Phys. Chem. Chem. Phys.* **2013**, *15*, 4329−4340.
(36) Hodnik, N.; Cherevko, S. Spot the difference at the nanoscale: identical location electron microscopy in electrocatalysis. *Curr. Opin. Electrochem.* **2019**, *15*, 73−82.
(37) Di Benedetto, F.; Camposeo, A.; Persano, L.; Laera, A. M.; Piscopiello, E.; Cingolani, R.; Tapfer, L.; Pisignano, D. Light-emitting nanocomposite CdS−polymer electrospun fibres via in situ nanoparticle generation. *Nanoscale* **2011**, *3*, 4234−4239.
(38) Jovanović, Z.; Pašti, I.; Kalijadis, A.; Jovanović, S.; Laušević, Z. Platinum-mediated healing of defective graphene produced by irradiating glassy carbon with a hydrogen ion-beam. *Mater. Chem. Phys.* **2013**, *141*, 27.
(39) Nataraj, S. K.; Yang, K. S.; Aminabhavi, T. M. Polyacrylonitrile-based nanofibers − A state-of-the-art review. *Prog. Polym. Sci.* **2012**, *37*, 487−513.
(40) Ferrari, A. C. Raman spectroscopy of graphene and graphite: disorder, electron−phonon coupling, doping and nonadiabatic effects. *Solid State Commun.* **2007**, *143*, 47−57.
(41) Trucano, P.; Chen, R. Structure of graphite by neutron diffraction. *Nature* **1975**, *258*, 136−137.
(42) Ruiz-Zepeda, F.; Gatalo, M.; Pavlišič, A.; Dražić, G.; Jovanovič, P.; Bele, M.; Gaberšček, M.; Hodnik, N. Atomically resolved anisotropic electrochemical shaping of nano-electrocatalyst. *Nano Lett.* **2019**, *19*, 4919−4927.
(43) Iwasita, T. Electrocatalysis of methanol oxidation. *Electrochim. Acta* **2002**, *47*, 3663−3674.
(44) Jovanovič, P.; Pavlišič, A.; Šelih, V. S.; Šala, M.; Hodnik, N.; Bele, M.; Hočevar, S.; Gaberšček, M. New insight into platinum dissolution from nanoparticulate platinum-based electrocatalysts using highly sensitive in situ concentration measurements. *ChemCatChem* **2014**, *6*, 449−453.
(45) Hodnik, N.; Bele, M.; Hočevar, S. New Pt-skin electrocatalysts for oxygen reduction and methanol oxidation reactions. *Electrochem. Commun.* **2012**, *23*, 125−128.
(46) Kim, C.; Park, S.-H.; Cho, J.-I.; Lee, D.-Y.; Park, T.-J.; Lee, W.-J.; Yang, K.-S. Raman spectroscopic evaluation of polyacrylonitrile-based carbon nanofibers prepared by electrospinning. *J. Raman Spectrosc.* **2004**, *35*, 928−933.
(47) Arshad, S. N.; Naraghi, M.; Chasiotis, I. Strong carbon nanofibers from electrospun polyacrylonitrile. *Carbon* **2011**, *49*, 1710−1719.
(48) Karacan, I.; Erzurumluoğlu, L. The effect of carbonization temperature on the structure and properties of carbon fibers prepared from poly(m-phenylene isophthalamide) precursor. *Fibers Polym.* **2015**, *16*, 1629−1645.
(49) Mittal, J.; Konno, H.; Inagaki, M.; Bahl, O. P. Denitrogenation behavior and tensile strength increase during carbonization of stabilized pan fibers. *Carbon* **1998**, *36*, 1327−1330.
(50) Mayrhofer, K. J. J.; Strmcnik, D.; Blizanac, B. B.; Stamenkovic, V.; Arenz, M.; Markovic, N. M. Measurement of oxygen reduction activities via the rotating disc electrode method: from Pt model surfaces to carbon-supported high surface area catalysts. *Electrochim. Acta* **2008**, *53*, 3181−3188.
(51) Breitwieser, M.; Klingele, M.; Vierrath, S.; Zengerle, R.; Thiele, S. Tailoring the membrane-electrode interface in PEM fuel cells: a review and perspective on novel engineering approaches. *Adv. Energy Mater.* **2018**, *8*, 1701257.
(52) Shakoorioskooie, M.; Menceloglu, Y. Z.; Unal, S.; Hayat Soytas, S. Rapid Microwave-Assisted Synthesis of Platinum Nanoparticles Immobilized in Electrospun Carbon Nanofibers for Electrochemical Catalysis. *ACS Appl. Nano Mater.* **2018**, *1*, 6236−6246.
(53) Ma, D.; Hu, B.; Wu, W.; Liu, X.; Zai, J.; Shu, C.; Tsega, T. T.; Chen, L.; Qian, X.; Liu, T. L. Highly active nanostructured CoS2/CoS heterojunction electrocatalysts for aqueous polysulfide/iodide redox flow batteries. *Nat. Commun.* **2019**, *10*, 3367.
(54) He, K.; Tadesse Tsega, T.; Liu, X.; Zai, J.; Li, X. H.; Liu, X.; Li, W.; Ali, N.; Qian, X. Utilizing the Space-Charge Region of the FeNi-LDH/CoP p-n Junction to Promote Performance in Oxygen Evolution Electrocatalysis. *Angew. Chem., Int. Ed.* **2019**, *58*, 11903−11909.
(55) Jovanovič, P.; Stojanovski, K.; Bele, M.; Dražić, G.; Koderman Podboršek, G.; Suhadolnik, L.; Gaberšček, M.; Hodnik, N. Methodology for Investigating Electrochemical Gas Evolution Reactions: Floating Electrode as a Means for Effective Gas Bubble Removal. *Anal. Chem.* **2019**, *91*, 10353−10356.

https://dx.doi.org/10.1021/acsanm.0c01945
ACS Appl. Nano Mater. 2020, 3, 9880−9888